HHS Public Access

Author manuscript

Neuroscience. Author manuscript; available in PMC 2024 October 01.

Published in final edited form as:

Neuroscience. 2023 October 01; 529: 172–182. doi:10.1016/j.neuroscience.2023.07.030.

Feed-forward activation of habenula cholinergic neurons by acetylcholine

Leeyup Chung[1], **Miao Jing**[3,4], **Yulong Li**[3,4], **Andrew R. Tapper**[1,*]

[1]Brudnick Neuropsychiatric Research Institute, Dept. of Neurobiology, University of Massachusetts Medical School, Worcester, MA, 01605, USA

[3]State Key Laboratory of Membrane Biology, Peking University School of Life Sciences; Peking-Tsinghua Center for Life Sciences; PKU-IDG/McGovern Institute for Brain Research, 100871 Beijing, China

[4]Chinese Institute for Brain Research, 102206 Beijing, China

Abstract

While the functional and behavioral role of the medial habenula (MHb) is still emerging, recent data indicate an involvement of this nuclei in regulating mood, aversion, and addiction. Unique to the MHb is a large cluster of cholinergic neurons that project to the interpeduncular nucleus and densely express acetylcholine receptors (AChRs) suggesting that the activity of these cholinergic neurons may be regulated by ACh itself. Whether endogenous ACh from within the habenula regulates cholinergic neuron activity has not been demonstrated. Supporting a role for ACh in modulating MHb activity, acetylcholinesterase inhibitors (ACEIs) increased the firing rate of MHb cholinergic neurons in mouse habenula slices, an effect blocked by AChR antagonists and mediated by ACh which was detected via expressing fluorescent ACh sensors in MHb in vivo. To test if cholinergic afferents innervate MHb cholinergic neurons, we used anterograde and retrograde viral tracing to identify cholinergic inputs. Surprisingly, tracing experiments failed to detect cholinergic inputs into the MHb, including from the septum, suggesting that MHb cholinergic neurons may release ACh within the MHb to drive cholinergic activity. To test this hypothesis, we expressed channelrhodopsin in a portion of MHb cholinergic neurons while recording from non-opsin-expressing neurons. Light pulses progressively increased activity of MHb cholinergic neurons indicating feed-forward activation driven by MHb ACh release. These data indicate MHb cholinergic neurons may utilize a unique feed-forward mechanism to synchronize and increase activity by releasing local ACh.

Introduction

The habenula complex is an epithalamic nucleus connecting limbic forebrain to midbrain (1). It is divided into medial habenula (MHb) and lateral habenula (LHb) with distinct

*Lead Contact, Correspondence to: andrew.tapper@umassmed.edu.

relay connections (2–4). Afferents from multiple septal nuclei terminate in MHb and efferents from bilateral MHb converges in the interpeduncular nucleus (IPN) of the midbrain which consists of multiple paired and unpaired sub-nuclei with a certain degree of distinct topography (3). The MHb is emerging as a brain area critical for addiction- and mood-associated behaviors among others (5–10), but how different afferent and efferent signals are processed within the MHb are largely unknown.

While the MHb consists of neurons with diverse gene expression, the nuclei contain a dense cluster of cholinergic neurons on the ventral side and substance P neurons on the dorsal side which project to central and lateral IPN, respectively. Interestingly, nAChR subunit genes and muscarinic receptors are widely and densely expressed in the MHb with the majority of nAChRs, uniquely expressed in (11, 12) cholinergic neurons in ventral MHb (13, 14). In neurons, functional nAChRs are expressed in soma, dendrites and axons (15–17). Although the role of nAChR signaling in MHb has not been fully elucidated, activation of nAChRs with exogenous nicotine in rodent MHb slices increases the spontaneous firing rate of ventral MHb cholinergic neurons in cell-attached recordings (13). In general, nicotine activation of MHb is associated with negative motivational signals, anxiety, and aversion (18–21). Nicotine addiction from smoking has received special attention because of strong nAChR expression (14). In addition, excitatory muscarinic receptors in medial habenula have been implicated in extinction of aversive stimuli upon repeated presentation in mouse models (22).

The density of AChR expression in general in MHb cholinergic soma/dendrites, specifically implies these neurons receive innervation from cholinergic inputs that release endogenous ACh into the nucleus (22)(23). Indeed, we previously reported anxiety-like behavior increases in mice after expression of hypersensitive α4* nAChR subunits in cholinergic MHb neurons, a phenotype reversed by nAChR antagonist infusion (24) indirectly suggesting endogenous ACh activates MHb cholinergic neurons via nAChR signaling. However, the source of the presumed cholinergic input is still emerging. While septal and/or brainstem cholinergic neurons have been hypothesized to innervate MHb, data supporting this idea are scant (5, 25, 26), although a recent study has implicated septal MHb inputs as a source of cholinergic innervation to MHb via muscarinic receptors (22). Thus, in this study, we tested the hypothesis that endogenous ACh is released in MHb with the goal of identifying both the function and source of cholinergic MHb innervation.

Methods

Animals.

All experiments followed guidelines for animal care and use by the Institutional Animal Care and Use Committee of the University of Massachusetts Medical School (UMMS). C57BL/6J (#000664), Chat::GFP (#007902), Chat::ChR2 (#014546), and Chat::Cre (#006410) mice were obtained from the Jackson Laboratory and were bred in the UMMS animal facility. All mice were group housed on 12 hour light/dark cycle (7 a.m. to 7 p.m.) with ad libitum food and water access.

Viral injection.

Mice (2–3 months old) were injected with a mixture of ketamine (100 mg/kg) and xylazine (10 mg/kg). Craniotomies were performed with a 0.4 mm drill bit at the target coordinates. Injection coordinates from bregma were (AP, ML, DV, angle): MHb (−1.7, −0.8, −3.1, 10°, 300 nL), LHb (−1.7, −1.1, −3.1, 10°, 300 nL), septum (+1.35, −0.8, −4.7, 10°, 1.0 μL), lateral dorsal tegmentum (LDT, −5.3, −0.4, −3.8, 1.0 μL), and IPN (−3.4, 0.8, −4.9, 10°, 1.0 μL). The angle of 10° was used to avoid major blood vessel in the midline. Injection speed was 30 – 100 nL / min using a Hamilton syringe (33-gauge) and pump (Stoelting). The injection needle was in place for another 5 to 10 min before slow withdrawal. Virus particles were obtained from Addgene: AAVrg-hSyn-DIO-EGFP (#50457-AAVrg), AAV2-hSyn-DIO-mCherry (#50459-AAV2), AAVrg-hSyn-eGFP-Cre (#50465-AAVrg), AAVrg-EF1a-DIO-ChR2-EYFP (#20298-AAVrg), AAV5-CAG-FLEX-GCaMP6m (100839-AAV5). AAV2-Ef1a-DIO-ChR2-eYFP (plasmids generously provided by K. Deisseroth) was packaged by the UMMS Viral Vector Core.

Brain slice preparation.

After pentobarbital injection (200 mg/kg, i.p.) and trans-cardial perfusion with NMDG slicing solution, brains were quickly extracted. Coronal brain slices (250 or 300 μm) were cut with a vibratome (Leica VT 1200) in ice-cold NMDG slicing solution, kept for 12 min in NMDG slicing solution at 34 °C, then moved to HEPES holding solution (25 °C) for at least 1 hour before the transfer to the recording chamber maintained at 25 °C in ACSF. NMDG slicing solution consisted of (in mM): NMDG 92, HEPES 20, $NaHCO_3$ 30, KCl 2.5, NaH_2PO_4 1.25, thiourea 2, Na-ascorbate 5, Na-pyruvate 3, glucose 25, $CaCl_2$ 0.5, $MgSO_4$ 10. HEPES holding solution included (in mM): NaCl 92, HEPES 20, $NaHCO_3$ 30, KCl 2.5, NaH_2PO_4 1.25, thiourea 2, Na-ascorbate 5, Na-pyruvate 3, glucose 25, $CaCl_2$ 2, $MgSO_4$ 2. ACSF consisted of (in mM): NaCl 125, KCl 2.5, NaH_2PO_4 1.25, glucose 11, $NaHCO_3$ 26, $MgCl_2$ 1.3, $CaCl_2$ 2.

Cell-attached recording.

The recording was performed in voltage clamp mode with holding potential of 0 mV. Pipette resistance (1B150F-4, WPI) was 2–4 MΩ. Na^+ based pipette solution contained (in mM): NaCl 145, KCl 2.5, $CaCl_2$ 2, $MgCl_2$ 1, HEPES 10, pH 7.4 adjusted with NaOH, osmolarity 290–294 mOsm (30). Data in Fig 1 was recorded from tight seal (>100 MΩ) patches, but all other patches were loose-seal (30~60 MΩ). Stable firing was monitored for 5–10 min before any treatments, otherwise cells were discarded.

Whole-cell recording.

Pipette solution contained (in mM): K-gluconate 126, KCl 4, HEPES 10, $MgCl_2$ 2, EGTA 1, $CaCl_2$ 0.1, MgATP 4, Na_2GFP 0.3, phosphocreatinine 10. Pipette resistance was 2–5 MΩ. To monitor post-synaptic potentials (PSPs), membrane potential was maintained below −55 mV with current injection to prevent unwanted spontaneous firing. ChR2 was activated with a 470 nm LED (pE-100, CoolLED) through the objective (60x/0.9 W) attached to the microscope (Olympus BX51WI). Pulse duration was 5 ms.

Signals from cell-attached and whole-cell recording were passed through DigiData 1440A, filtered (3 kHz low-pass, Bessel) and digitized at 20 KHz (Multiclamp 700B, Molecular Devices), and recorded with pClamp software (version 11, Molecular Devices). Series resistance was not compensated.

Spontaneous PSP quantification.

To quantify the PSPs, power spectrum analysis was used with Clampfit software (version 10.7). Importantly, power spectrum analysis was used because it reflects unbiased differences in signal and provides an objective way to analyze membrane potential fluctuations.

In Fig. 1H and I, the interval for power calculation was the last 10 s from a 30 s sweep. The powers from 5 sweeps (2.5 min) were averaged. Subsequently, the power after mecamylamine application was normalized by the power before mecamylamine application. In Fig. S1D and F, power was calculated in the interval of the last 16 s from a 20 s sweep and values from 6 sweeps (2 min duration) were averaged. In each cell, the averaged power after antagonist application (2 min) was normalized with that before the antagonist application (2 min) to remove basal PSP differences across cells.

ACh3.0 fluorescence imaging in slice.

To express the ACh3.0 sensor in MHb neurons, AAV of ACh3.0 (AAV9-hSyn-ACh3.0; YL10002-AAV9, WZ Bioscience) was injected into IPN (−3.4, −0.8, −4.9, 10°; 1.0 μL). ACh3.0 fluorescence was excited with 470 nm LED (CoolLED) and images were recorded with a digital camera (ASI183MM Pro) and software (μ-manager 1.4) at 1 Hz. Intensity was quantified with ImageJ.

Fiber Photometry.

Under anesthesia (ketamine/xylazine), an optic fiber (Doric MFC_200/230–0.48_4mm_SMR_FLT) was positioned at MHb using coordinates from bregma (AP, ML, DV, angle) −1.70, −0.75, −2.80, 10°. Imaging was done with Doric system (FPS_1S_405/GFP_400–0.57). Excitation LED was 405 nm (12 μW, 208.616 Hz) and 465 nm (28 μW, 530.481 Hz). Emitted signal was detected with a 430 and 525 nm photoreceiver. Sample signal (12.0 kS/s) was decimated by a factor of 50 and saved. For analysis, original signal was low-pass filtered (6 Hz), then saved into 1 sec bin. To account for slow drift in the signal, data 10 min before nicotine was fitted with linear regression. Data afterward was adjusted with the regression parameters. Mean and SD calculated before nicotine was used to calculate the z-score during the whole period. For drug treatment, saline, physostigmine (0.5 mg/kg) or nicotine (1.5 mg/kg) was injected subcutaneously on the dorsal side. After the recording, the optic fiber was fixed with dental cement (Metabond, Parkell) and location was verified after brain isolation one week post-surgery.

Immunohistochemistry.

Retrograde ChR2 (AAVrg-EF1a-DIO-hChR2(H134R)-EYFP; Addgene 20298-AAVrg) was injected into IPN of Chat::Cre mice (2–4 months old). After more than 4 weeks, mice were perfused with phosphate buffer saline (PBS), then with 4% paraformaldelyde (PFA) in

PBS. Extracted brains were kept in PFA overnight followed by sucrose (30%) for 2 days. Cryoprotected brains (OCT) were sectioned (40 μm for antibody staining or 80 μm for virus expression check) using a cryostat (Leica CM3050 S). After washing with 0.3% Triton-X in PBS (TBS, 3x, 10 min) and blocking for 1 hour (BlockOne 10% in TBS), slices were incubated in primary antibody (1:500, rabbit anti-VAChT, sysy 139 103) for more than 18 hours at 4 °C. After washing (TBS, 3x, 10 min), slices were incubated in secondary antibody (1:1000, donkey anti-rabbit Alexa Fluor 594; A212071) with DAPI overnight at 4 °C. Slices were mounted, cover-slipped with antifading agent (Mowiol, Sigma), and imaged via a fluorescence microscope (Zeiss, Axiovert 200M with X-cite 120 fluorescence illumination system, 20x objective).

Statistics.

Normality was tested with D'Agostino-Pearson omnibus test or, if D'Agostino-Pearson omnibus test were not applicable due to small sample number, Shapiro-Wilk test was used. Data were expressed as mean ± standard error of the mean (SEM) or median with range. Used tests were paired or unpaired t-test, repeated one-way analysis of variance (ANOVA), and repeated two-way ANOVA. For post-hoc multiple comparisons test, Tukey's test was used. Significance was set at $P<0.05$ or p-values were noted. Statistical tests were run using Prism 7 (Graphpad Sofware Inc.).

Results

Endogenous ACh modulates neuronal activity in MHb

If ACh is released inside MHb, it will be rapidly hydrolyzed by acetylcholinesterase (AChE) likely preventing observations of endogenous ACh modulating MHb neuron firing rate in epithalamic slices (13, 29). To test this hypothesis, we bath applied AChE inhibitors (AChEI, neostigmine and physostigmine, 20 μM) while recording from MHb cholinergic neurons in cell-attached mode. Recordings were made in slices from choline acetyltransferase (ChAT)::GFP mice to allow for identification of cholinergic neurons (Fig. 1A). AChEIs significantly increased spontaneous firing rate of MHb cholinergic neurons compared to ACSF (1.67 ± 0.11 n=9) (Fig. 1A, B, C). We further tested the effects of AChEIs on MHb cholinergic firing rate in the presence of AMPA, NMDA, $GABA_A$, and $GABA_B$ antagonists (NBQX 10 μM, CPP 10 μM, SR95531 10 μM, CGP52432 5 μM), to block glutamate and GABA receptor signaling. AChEI-mediated increases in firing persisted in the presence of the antagonists but were significantly blocked by preapplication of AChR antagonists (mecamylamine (Mec) 3 μM and atropine 1 μM, to block nAChRs and muscarinic receptors, respectively) indicating the effects of the AChEIs were mediated through cholinergic receptor signaling (Fig. 1D, E, F). AChEIs also increased activity of ventral MHb neurons in C57BL/6J mice, an effect similarly sensitive to AChR antagonists demonstrating results from ChAT::GFP mice were not influenced by the ChAT(BAC)-eGFP transgene (Fig. S1A, B). These data indicate that the firing increases observed after AChEI application was mediated by elevated endogenous ACh in the MHb.

If ACh release occurs spontaneously in MHb, then release facilitation in the absence of AChEIs could be possible by strongly activating cholinergic release sites. To test this

hypothesis, we recorded from MHb neurons in whole-cell current clamp mode in slices from ChAT::channelrhodopsin-2 (ChR2) mice while repeatedly stimulating neurons with blue light (5 ms pulse, 20 Hz, 5 s, 30 s intervals/sweep) in the presence of receptor antagonists (NBQX, CPP, SR95531, CGP52432) and 4-AP (Fig. 1G, H, I) without AChEI. Importantly, bath application of the nAChR antagonist, mecamylamine (Mec, 3 μM) significantly reduced power of PSPs (Fig. 1I) while repeated stimulation without Mec did not cause reduction in post-synaptic potentials (PSPs, Fig. S1C, D) suggesting specificity for Mec in PSP reduction. In addition, AChR-antagonist-sensitive PSPs were also apparent without stimulation in the presence of AChEIs (Fig. S1E, F). Finally, the magnitude of PSPs, as measured by area under the curve, was significantly increased by the presence of an additional AChEI, galantamine in C57BL/6J mice (Fig. S1G, H, I). Taken together, these data suggest that ACh release sites may be present inside MHb and the release itself can be manipulated by stimulation of cholinergic neurons.

ACh detection in MHb in vivo with the ACh3.0 fluorescent sensor

To directly record the dynamics of ACh in the MHb, we expressed a recently developed G-protein coupled receptor-based ACh sensor, $GRAB_{ACh3.0}$ (ACh3.0), which increase its fluorescence upon ACh binding (31). ACh3.0 was packaged into AAV9 and viral particles were injected into the IPN of C57BL/6J mice allowing for imaging of the IPN, as a positive control, as well as MHb, which is infected through retrograde transport (Fig. 2A). In IPN slices, bath application of an AChEI significantly increased ACh3.0 fluorescence signal which was blocked in the presence of atropine which antagonizes the sensor as it has an M3 receptor backbone (Fig. S2A, B).

To test if ACh at the MHb could be detected in vivo, we expressed ACh3.0 sensors in MHb as above and used fiber photometry to detect changes in fluorescence in anesthetized mice (Fig. 2A). To activate MHb cholinergic neurons, mice were pre-injected with saline or physostigmine followed 5 min later with an s.c. injection of 1.5 mg/kg nicotine and changes in fluorescence signal at 465 nm were acquired. After a saline injection, nicotine increased fluorescence in MHb which was potentiated by physostigmine indicating an increase in endogenous ACh in the MHb (Fig. 2B). To verify that nicotine, and consequently, ACh release resulted in activation of MHb cholinergic neurons, we expressed GCaMP6m in MHb cholinergic neurons of ChAT::Cre mice and performed fiber photometry as above (Fig. 2C). Nicotine significantly increased activation of MHb cholinergic neurons (Fig. 2D).

Local MHb ACh release activates neurons by a feed-forward mechanism.

To identify cholinergic afferents as a potential source of ACh release in MHb, we injected a Cre-dependent viral-mediated retrograde tracer, AAV2-retro-eGFP (AAV2rg-hSyn-DIO-EGFP) into the MHb of ChAT::Cre mice (Fig. 3A). To confirm proper injection into the MHb, we co-injected an anterograde marker (AAV2-hSyn-DIO-mCherry, n=5 brains). Injection of AAV2-retro-eGFP targeted the MHb as indicated by marker virus. In subsequent analysis of known cholinergic-rich areas (also verified by analysis of ChAT::GFP mice, Fig. S3A) hypothesized to project to the MHb including the medial septum (MS), the nucleus of diagonal band (NDB), the bed nucleus of anterior commissure (BAC), and the triangular septum (TS), cholinergic projections to the MHb were not detected (Fig. 3B). To confirm

these negative findings, we also injected a Cre-dependent anterograde tracer into MS and NDB of ChAT::Cre mice and observed no discernable inputs into the MHb (Fig 3C). In contrast, analysis of the laterodorsal tegmental nucleus (LDT) in ChAT::Cre mice injected with AAV2-retro-eGFP in the MHb revealed a small group of labeled neurons (n=2–4 per slice) visible in 2 of 5 brains with no cells detected in the other 3 brains (data not shown). Because the LDT is a cholinergic area projecting to the LHb, axonal terminals from the LDT to the LHb could have inadvertently been infected with AAV2-retro-eGFP. To test this, we targeted the LHb directly with AAV2-retro-eGFP in ChAT::Cre mice. We observed labeled neurons in the LDT (n=4–14/slice, Fig. S3B). To further confirm LDT→LHb cholinergic terminals, anterograde virus (AAV2-hSyn-DIO-mCherry) was injected into LDT of Chat::Cre mice. Axons from LDT were visible in LHb, but not in MHb (Fig. 3D). These data suggest that, in ChAT::Cre mice, the MHb does not receive significant cholinergic innervation from afferents, rather ACh release may be generated by MHb cholinergic neurons themselves.

To test this hypothesis, we sought to selectively stimulate MHb cholinergic neurons while recording AP firing rate from non-stimulated cholinergic neurons to measure functional effects of potential local ACh release. To achieve this goal, we injected AAV2-retro-ChR2 (AAVrg-EF1a-DIO-ChR2-EYFP) virus into the IPN of ChAT::Cre mice which resulted in a portion of MHb cholinergic neurons expressing ChR2 (Fig. 4A). To detect local ACh-mediated changes in firing rate, action potentials were monitored with cell-attached recording from ChR2-negative neurons located near ChR2-positive cholinergic neurons which were readily discernable based on lack or presence of eYFP and light-evoked APs, respectively (Fig 4B). We monitored firing rate of ChR2-negative neurons in response to sweeps of 20 sec 50 Hz light stimulation based on previous reports indicating higher frequency stimulation is necessary for ACh release from MHb cholinergic terminals in the IPN (32). Remarkably, compared to baseline, ChR2-negative neurons steadily increased their firing rate in response to three consecutive light pulses (Fig. 4C, D, E). To test if increased firing rate was, indeed, mediated by ACh, we repeated the experiment in the presence of AChR antagonists (Mec and atropine). Addition of AChR antagonists reduced the stimulation-mediated firing increase (Fig. 4E).

Discussion

The MHb is emerging as a key regulator in mood, response to aversive stimuli, and addiction, however the neurotransmitter systems and signaling mechanisms in the MHb are still emerging. The MHb contains a dense cluster of cholinergic neurons on the ventral side that are unique in that they have the highest expression of nAChR in the brain, in addition to excitatory muscarinic receptors suggesting that they are robustly regulated by ACh and cholinergic signaling. Our data in habenula mouse brain slices and in vivo have identified that ACh is released and able to modulate activity of MHb cholinergic neurons.

Previous data in habenula rodent slices indicated that nAChR antagonists (i.e., mecamylamine), alone, did not affect the spontaneous firing rate of MHb cholinergic neurons likely due to an additional requirement of muscarinic receptor modulation of firing rate, negligible ACh release in slices because of severed cholinergic inputs, and/or

high expression of acetylcholinesterase which rapidly hydrolyzes ACh (13, 29). The latter hypothesis predicts that inhibition of AChE activity will allow endogenous ACh to activate AChRs thereby modulating neuronal firing. Consistent with this prediction, our data show AChEIs increased firing rate (Fig 1) in a similar pattern to exogenous effects of the nAChR agonist, nicotine (13, 14, 34, 35). AChEIs increased post-synaptic potentials from whole-cell recordings of MHb cholinergic neurons corroborating the conclusion from cell-attached recordings of ACh-mediated increase in action potential firing. Effects of AChEIs on PSPs persisted even in the presence of glutamate and GABA receptor antagonists, as well as TTX, and were sensitive to blockade by AChR antagonists. Importantly, optical stimulation of cholinergic neurons increased PSPs via nAChRs (Fig. 1 and S1), which, to our knowledge is the first demonstration of nAChR-mediated PSPs in the habenula (36, 37), although the sufficiency of these small, nAChR-mediated PSPs in increasing firing rate was not examined further. While previous work in rat MHb demonstrated that spontaneous EPSPs were inhibited by AMPA antagonist or TTX (38), AChR antagonists were not tested. Prior studies also tested the effects of exogenous ACh (10 μM) application on inward current and intracellular calcium, but did not analyze post-synaptic potentials/currents (39). One potential concern with the interpretation of these data is that effects of AChEIs and ChR2 stimulation on MHb cholinergic neuron activity were performed in ChAT::GFP and ChAT::ChR2 mice which may have altered cholinergic signaling due to increased vesicular choline transporter expression. However, the main effects of AChEI in MHb slices were replicated in C57BL/6J mice (Figure S1A, B, G, H, I). In addition, feed forward activation of MHb cholinergic neurons were demonstrated using ChAT-IRES-Cre hemizygous animals (Jackson strain #006410) which are similar to wild-type mice in protein expression and behavioral assessments (Chen E et al., 2018).

While our physiological and pharmacology data support a role for endogenous ACh in modulating MHb cholinergic neurons, we further tested the presence of endogenous ACh using the ACh GRAB fluorescent sensor, ACh3.0, which allows for imaging of ACh levels in a given brain area where it is expressed (40). ACh imaging reflects the binding of ACh molecule to the ACh3.0 sensor distributed in the imaged region. Our combined physiology and ACh3.0 fluorescence imaging results indicate the presence of endogenous ACh in MHb which can regulate cholinergic neuron activity.

Detailed functional characterization of cholinergic MHb afferents is incomplete and not all afferents have been definitively identified. A prevailing hypothesis is that MHb receives cholinergic input from the basal forebrain through the stria medullaris and particularly the septum which provides dense innervation of MHb via GABAergic and glutamatergic projections (2, 7, 41) (21, 27–29). While previous work in generating a whole-brain atlas of the cholinergic system did not identify cholinergic input to MHb(42), a recent study used AAV delivery of eGFP and opsins under the control of the ChAT promoter in C57BL/6J mice to label and manipulate putative septal cholinergic neurons that project to and innervate the MHb. The authors concluded that cholinergic septum inputs to MHb are engaged by aversive stimuli and contribute to aversion-generalization formation and extinction (22). Surprisingly, using Cre-dependent anterograde and retrograde viral tracers in combination with ChAT::Cre mice, we failed to detect robust projections from basal forebrain. One caveat to our tracing approach is that it utilized the ChAT::Cre mouse line, thus we cannot

rule out that cholinergic circuits in this line may not completely recapitulate those in non-genetically engineered, wild-type mice as the ChAT::Cre may exhibit reduced ChAT expression (43). However, this is less of a concern since we used heterozygous ChAT::Cre mice. In addition, we verified known cholinergic projections from the LDT to the LHb and observed septal cholinergic inputs to the hippocampus (Fig. 3C) in these animals as a positive control. We also note that viral manipulations in Mu et al., utilized AAV9 which likely spread to cholinergic neurons within the MHb itself making precise identification and opto/chemogenetic manipulation of putative septum cholinergic MHb input difficult. Future experiments will be needed to confirm septal cholinergic innervation of the MHb. We also failed to identify LDT cholinergic neuron projections to the MHb, although cholinergic LDT→LHb projections were detected, as discussed above, consistent with reports that midbrain cholinergic neurons in PPT/LDT project to thalamus in general (44, 45). Taken together, our data indicate that a cholinergic septal input to the MHb, if present, is weak.

Regardless of whether afferent cholinergic inputs to MHb exist, we hypothesized that MHb cholinergic neurons may be a source of ACh. By injecting AAV2-retro-ChR2 into IPN of Chat::Cre mice, expression of ChR2 in a portion of MHb cholinergic neurons was achieved allowing for recording of ChR2-negative neurons while stimulating ChR2-positive neurons. To stimulate the ACh release, we used similar protocols (50 Hz, 20 sec) used to stimulate ACh release from MHb cholinergic terminals in the IPN (32). Remarkably, optically stimulating ChR2-positive cholinergic neurons steadily increased the firing rate of ChR2-negative cholinergic neurons indicating that MHb neurons are not functionally separate from each other. In a previous study, action potential-dependent EPSPs were speculated to come from neighboring MHb cells, but the possibility was not tested (Kim and Chang, 2005). In addition, ACh receptor antagonists revealed that endogenous ACh from MHb facilitates excitatory communication between MHb neurons by AChR signaling providing a unique mechanism of feedforward activation between MHb cholinergic neurons.

Future studies should elucidate how feed-forward activation of MHb cholinergic neurons by ACh may modulate behavior. Hints may be gleaned from previous work by our lab where alpha4 nAChR subunits harboring a gain-of-function mutation that rendered nAChRs hypersensitive to ACh were expressed in MHb cholinergic neurons (24). Mice expressing the gain-of-function nAChRs exhibited increased anxiety-like behavior compared to control mice and this phenotype was reversed by blocking the receptor with a nAChR antagonist. Similarly, chronic nicotine upregulates nAChR in MHb cholinergic neurons and withdrawal from nicotine increases anxiety, an effect potentially mediated by increased cholinergic signaling in MHb cholinergic neurons. These results indicate that the increased ACh neurotransmission and feed forward activation of MHb cholinergic neurons may contribute to anxiety-related behaviors.

Overall conclusion:

In summary, our data indicate that MHb cholinergic neurons may release ACh during spontaneous firing. The released ACh is kept at very low level by AChE, but under certain conditions the released ACh may overcome the hydrolysis barrier to activate receptors, acting as excitatory input to neighboring cholinergic neurons. This positive feedback (or

feed forward) activation can amplify and likely synchronize cholinergic neuron activity within the MHb. This unique mechanism may be critical for one or more aspect anxiety-like and/or addiction-associated behavior.

Supplementary Material

Refer to Web version on PubMed Central for supplementary material.

ACKNOWLEDGEMENTS

We thank Anthony Sacino and Michael Gorczyca for technical support and Karl Deisseroth for optogenetic plasmids. This work was supported by the National Institute on Drug Abuse award number DA041482 (A.R.T.) and DA047678 (A.R.T.). The content is solely the responsibility of the authors and does not necessarily represent the official views of the National Institutes of Health.

References

1. Sutherland RJ (1982) The dorsal diencephalic conduction system: a review of the anatomy and functions of the habenular complex. Neuroscience and biobehavioral reviews 6, 1–13 [PubMed: 7041014]
2. Herkenham M, and Nauta WJ (1977) Afferent connections of the habenular nuclei in the rat. A horseradish peroxidase study, with a note on the fiber-of-passage problem. The Journal of comparative neurology 173, 123–146 [PubMed: 845280]
3. Herkenham M, and Nauta WJ (1979) Efferent connections of the habenular nuclei in the rat. J Comp Neurol 187, 19–47 [PubMed: 226566]
4. Hu H, Cui Y, and Yang Y. (2020) Circuits and functions of the lateral habenula in health and in disease. Nature reviews. Neuroscience 21, 277–295 [PubMed: 32269316]
5. Antolin-Fontes B, Ables JL, Görlich A, and Ibañez-Tallon I. (2015) The habenulo-interpeduncular pathway in nicotine aversion and withdrawal. Neuropharmacology 96, 213–222 [PubMed: 25476971]
6. Lee HW, Yang SH, Kim JY, and Kim H. (2019) The Role of the Medial Habenula Cholinergic System in Addiction and Emotion-Associated Behaviors. Frontiers in psychiatry 10, 100 [PubMed: 30873055]
7. McLaughlin I, Dani JA, and De Biasi M. (2017) The medial habenula and interpeduncular nucleus circuitry is critical in addiction, anxiety, and mood regulation. Journal of neurochemistry 142 Suppl 2, 130–143 [PubMed: 28791703]
8. Molas S, Zhao-Shea R, Liu L, DeGroot SR, Gardner PD, and Tapper AR (2017) A circuit-based mechanism underlying familiarity signaling and the preference for novelty. Nat Neurosci 20, 1260–1268 [PubMed: 28714952]
9. DeGroot SR, Zhao-Shea R, Chung L, Klenowski PM, Sun F, Molas S, Gardner PD, Li Y, and Tapper AR (2020) Midbrain Dopamine Controls Anxiety-like Behavior by Engaging Unique Interpeduncular Nucleus Microcircuitry. Biol Psychiatry 88, 855–866 [PubMed: 32800629]
10. Klenowski PM, Zhao-Shea R, Freels TG, Molas S, and Tapper AR (2021) Dynamic activity of interpeduncular nucleus GABAergic neurons controls expression of nicotine withdrawal in male mice. Neuropsychopharmacology
11. Hashikawa Y, Hashikawa K, Rossi MA, Basiri ML, Liu Y, Johnston NL, Ahmad OR, and Stuber GD (2020) Transcriptional and Spatial Resolution of Cell Types in the Mammalian Habenula. Neuron 106, 743–758 e745 [PubMed: 32272058]
12. Wallace ML, Huang KW, Hochbaum D, Hyun M, Radeljic G, and Sabatini BL (2020) Anatomical and single-cell transcriptional profiling of the murine habenular complex. eLife 9
13. Gorlich A, Antolin-Fontes B, Ables JL, Frahm S, Slimak MA, Dougherty JD, and Ibanez-Tallon I. (2013) Reexposure to nicotine during withdrawal increases the pacemaking activity of cholinergic habenular neurons. Proc Natl Acad Sci U S A 110, 17077–17082 [PubMed: 24082085]

14. Shih PY, Engle SE, Oh G, Deshpande P, Puskar NL, Lester HA, and Drenan RM (2014) Differential expression and function of nicotinic acetylcholine receptors in subdivisions of medial habenula. J Neurosci 34, 9789–9802 [PubMed: 25031416]
15. Arvin MC, Jin XT, Yan Y, Wang Y, Ramsey MD, Kim VJ, Beckley NA, Henry BA, and Drenan RM (2019) Chronic Nicotine Exposure Alters the Neurophysiology of Habenulo-Interpeduncular Circuitry. J Neurosci 39, 4268–4281 [PubMed: 30867261]
16. Banala S, Arvin MC, Bannon NM, Jin XT, Macklin JJ, Wang Y, Peng C, Zhao G, Marshall JJ, Gee KR, Wokosin DL, Kim VJ, McIntosh JM, Contractor A, Lester HA, Kozorovitskiy Y, Drenan RM, and Lavis LD (2018) Photoactivatable drugs for nicotinic optopharmacology. Nature methods 15, 347–350 [PubMed: 29578537]
17. Passlick S, Thapaliya ER, Chen Z, Richers MT, and Ellis-Davies GCR (2018) Optical probing of acetylcholine receptors on neurons in the medial habenula with a novel caged nicotine drug analogue. The Journal of physiology 596, 5307–5318 [PubMed: 30222192]
18. Picciotto MR, and Kenny PJ (2013) Molecular mechanisms underlying behaviors related to nicotine addiction. Cold Spring Harbor perspectives in medicine 3, a012112
19. Molas S, DeGroot SR, Zhao-Shea R, and Tapper AR (2017) Anxiety and Nicotine Dependence: Emerging Role of the Habenulo-Interpeduncular Axis. Trends Pharmacol Sci 38, 169–180 [PubMed: 27890353]
20. Zhao-Shea R, DeGroot SR, Liu L, Vallaster M, Pang X, Su Q, Gao G, Rando OJ, Martin GE, George O, Gardner PD, and Tapper AR (2015) Increased CRF signalling in a ventral tegmental area-interpeduncular nucleus-medial habenula circuit induces anxiety during nicotine withdrawal. Nature communications 6, 6770
21. Yamaguchi T, Danjo T, Pastan I, Hikida T, and Nakanishi S. (2013) Distinct roles of segregated transmission of the septo-habenular pathway in anxiety and fear. Neuron 78, 537–544 [PubMed: 23602500]
22. Mu R, Tang S, Han X, Wang H, Yuan D, Zhao J, Long Y, and Hong H. (2022) A cholinergic medial septum input to medial habenula mediates generalization formation and extinction of visual aversion. Cell reports 39, 110882
23. Miwa JM, Freedman R, and Lester HA (2011) Neural systems governed by nicotinic acetylcholine receptors: emerging hypotheses. Neuron 70, 20–33 [PubMed: 21482353]
24. Pang X, Liu L, Ngolab J, Zhao-Shea R, McIntosh JM, Gardner PD, and Tapper AR (2016) Habenula cholinergic neurons regulate anxiety during nicotine withdrawal via nicotinic acetylcholine receptors. Neuropharmacology 107, 294–304 [PubMed: 27020042]
25. Woolf NJ, and Butcher LL (2011) Cholinergic systems mediate action from movement to higher consciousness. Behavioural brain research 221, 488–498 [PubMed: 20060422]
26. Contestabile A, and Fonnum F. (1983) Cholinergic and GABAergic forebrain projections to the habenula and nucleus interpeduncularis: surgical and kainic acid lesions. Brain research 275, 287–297 [PubMed: 6626983]
27. Qin C, and Luo M. (2009) Neurochemical phenotypes of the afferent and efferent projections of the mouse medial habenula. Neuroscience 161, 827–837 [PubMed: 19362132]
28. Otsu Y, Lecca S, Pietrajtis K, Rousseau CV, Marcaggi P, Dugué GP, Mailhes-Hamon C, Mameli M, and Diana MA (2018) Functional Principles of Posterior Septal Inputs to the Medial Habenula. Cell reports 22, 693–705 [PubMed: 29346767]
29. Choi K, Lee Y, Lee C, Hong S, Lee S, Kang SJ, and Shin KS (2016) Optogenetic activation of septal GABAergic afferents entrains neuronal firing in the medial habenula. Scientific reports 6, 34800 [PubMed: 27703268]
30. Alcami P, Franconville R, Llano I, and Marty A. (2012) Measuring the firing rate of high-resistance neurons with cell-attached recording. The Journal of neuroscience : the official journal of the Society for Neuroscience 32, 3118–3130
31. Jing M, Li Y, Zeng J, Huang P, Skirzewski M, Kljakic O, Peng W, Qian T, Tan K, Zou J, Trinh S, Wu R, Zhang S, Pan S, Hires SA, Xu M, Li H, Saksida LM, Prado VF, Bussey TJ, Prado MAM, Chen L, Cheng H, and Li Y. (2020) An optimized acetylcholine sensor for monitoring in vivo cholinergic activity. Nature methods 17, 1139–1146 [PubMed: 32989318]

32. Ren J, Qin C, Hu F, Tan J, Qiu L, Zhao S, Feng G, and Luo M. (2011) Habenula “cholinergic” neurons co-release glutamate and acetylcholine and activate postsynaptic neurons via distinct transmission modes. Neuron 69, 445–452 [PubMed: 21315256]
33. Arvidsson U, Riedl M, Elde R, and Meister B. (1997) Vesicular acetylcholine transporter (VAChT) protein: a novel and unique marker for cholinergic neurons in the central and peripheral nervous systems. The Journal of comparative neurology 378, 454–467 [PubMed: 9034903]
34. Lee C, Lee S, Woo C, Kang SJ, Kim Kwon Y, and Shin KS (2018) Differential regulation of neuronal excitability by nicotine and substance P in subdivisions of the medial habenula. Animal cells and systems 22, 165–171 [PubMed: 30460094]
35. Shih PY, McIntosh JM, and Drenan RM (2015) Nicotine Dependence Reveals Distinct Responses from Neurons and Their Resident Nicotinic Receptors in Medial Habenula. Mol Pharmacol 88, 1035–1044 [PubMed: 26429939]
36. Bandyopadhyay S, Sutor B, and Hablitz JJ (2006) Endogenous acetylcholine enhances synchronized interneuron activity in rat neocortex. Journal of neurophysiology 95, 1908–1916 [PubMed: 16338999]
37. Yorgason JT, Zeppenfeld DM, and Williams JT (2017) Cholinergic Interneurons Underlie Spontaneous Dopamine Release in Nucleus Accumbens. The Journal of neuroscience : the official journal of the Society for Neuroscience 37, 2086–2096
38. Kim U, and Chang SY (2005) Dendritic morphology, local circuitry, and intrinsic electrophysiology of neurons in the rat medial and lateral habenular nuclei of the epithalamus. The Journal of comparative neurology 483, 236–250 [PubMed: 15678472]
39. Lester RA (2004) Activation and desensitization of heteromeric neuronal nicotinic receptors: implications for non-synaptic transmission. Bioorganic & medicinal chemistry letters 14, 1897–1900
40. Jing M, Zhang P, Wang G, Feng J, Mesik L, Zeng J, Jiang H, Wang S, Looby JC, Guagliardo NA, Langma LW, Lu J, Zuo Y, Talmage DA, Role LW, Barrett PQ, Zhang LI, Luo M, Song Y, Zhu JJ, and Li Y. (2018) A genetically encoded fluorescent acetylcholine indicator for in vitro and in vivo studies. Nature biotechnology 36, 726–737
41. Woolf NJ (1991) Cholinergic systems in mammalian brain and spinal cord. Progress in neurobiology 37, 475–524 [PubMed: 1763188]
42. Li X, Yu B, Sun Q, Zhang Y, Ren M, Zhang X, Li A, Yuan J, Madisen L, Luo Q, Zeng H, Gong H, and Qiu Z. (2018) Generation of a whole-brain atlas for the cholinergic system and mesoscopic projectome analysis of basal forebrain cholinergic neurons. Proceedings of the National Academy of Sciences of the United States of America 115, 415–420 [PubMed: 29259118]
43. Chen E, Lallai V, Sherafat Y, Grimes NP, Pushkin AN, Fowler JP, and Fowler CD (2018) Altered Baseline and Nicotine-Mediated Behavioral and Cholinergic Profiles in ChAT-Cre Mouse Lines. J Neurosci 38, 2177–2188 [PubMed: 29371319]
44. Mena-Segovia J, and Bolam JP (2017) Rethinking the Pedunculopontine Nucleus: From Cellular Organization to Function. Neuron 94, 7–18 [PubMed: 28384477]
45. Huerta-Ocampo I, Hacioglu-Bay H, Dautan D, and Mena-Segovia J. (2020) Distribution of Midbrain Cholinergic Axons in the Thalamus. eNeuro 7
46. Gilmor ML, Nash NR, Roghani A, Edwards RH, Yi H, Hersch SM, and Levey AI (1996) Expression of the putative vesicular acetylcholine transporter in rat brain and localization in cholinergic synaptic vesicles. The Journal of neuroscience : the official journal of the Society for Neuroscience 16, 2179–2190 [PubMed: 8601799]
47. Frahm S, Antolin-Fontes B, Görlich A, Zander JF, Ahnert-Hilger G, and Ibañez-Tallon I. (2015) An essential role of acetylcholine-glutamate synergy at habenular synapses in nicotine dependence. eLife 4, e11396

Highlights

- Endogenous acetylcholine modulates medial habenula neuronal activity.
- Acetylcholine can be detected in medial habenula *in vivo*.
- Acetylcholine release from medial habenula can elicit feed-forward activation.

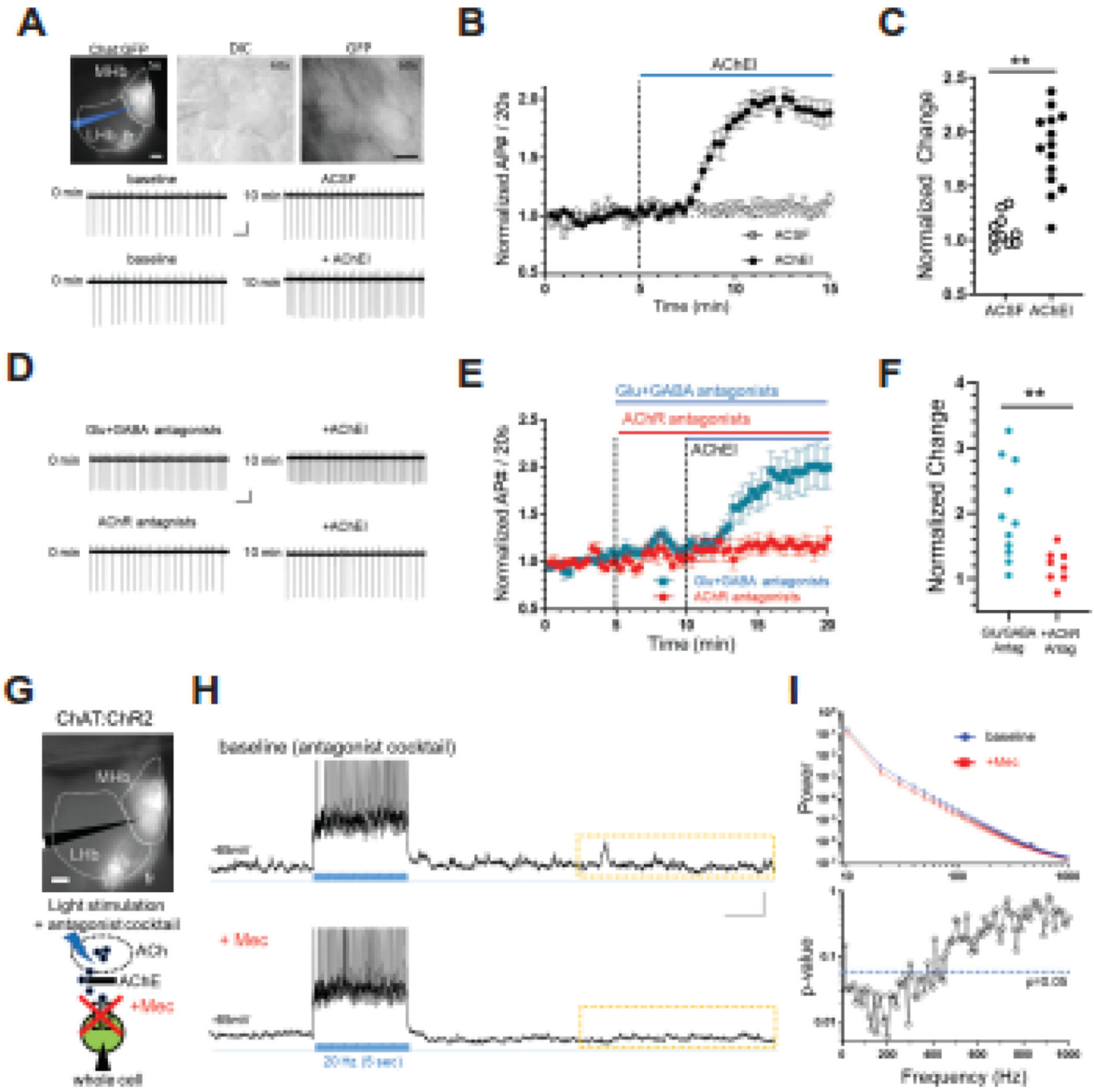

Figure 1. Endogenous ACh can drive cholinergic neuron activity in MHb via AChR signaling.

A. Photomicrographs depicting the recording area in a habenula slice from a ChAT::GFP mouse under fluorescence microscopy (top, left, scale bar: 100 μm), at higher magnification under DIC microscopy (top, middle) and fluorescence microscopy (top, right, scale bar: 10 μm). The patch pipette is depicted in blue (top, left). Representative cell-attached recording from cholinergic habenula neurons at baseline (middle, left) and after 10 min control solution (ACSF, middle right). Representative cell-attached recording from cholinergic habenula neurons at baseline (bottom, left) and after 10 min bath perfusion with acetylcholinesterase inhibitor physostigmine and neostigmine (AChEIs, bottom right). Scale

bar: 1 sec, 10 pA. **B.** Average number of spontaneous APs in response to bath application (denoted by the blue bar) of AChEIs or control ACSF. Each data point represents the normalized average AP during 20 s intervals. **C.** Scatter plot of AP frequency change at the end of 10 min application of AChEIs compared to baseline (ACSF, 1.09 ± 0.04, n=10; AChEI, 1.88 ± 0.10, n=15; unpaired t-test, t=6.13, df=23, **p<0.0001). **D.** Representative cell-attached recording from cholinergic habenula neurons in the presence of iGluR (AMPA type, NBQX 10 μM; NMDA type, CPP 10 μM) and GABAR (GABA-A type, SR95531 10μM; GABA-B type, CGP52432 5 μM) antagonists before (top, left) and after (top, right) application of AChEIs. Bottom panels depict representative cell-attached recordings in the presence of AChR antagonists (nAChR, mecamylamine 3 μM; mAChR, atropine 1 μM) before (bottom, left) and after (bottom, right) AChEI application. Scale bar: 1 sec, 10 pA. **E.** Average number of APs in response to bath application (denoted by the blue bar) of AChEIs in the presence of iGluR and GABAR antagonists or AChR antagonists. Each data point represents the normalized average AP during 20 s intervals. **F.** Scatter plot of AP frequency change at the end of 10 min application of AChEIs in the presence of iGluR and GABAR antagonists or AChR antagonists (iGluR and GABAR antagonists, 2.00 ± 0.22, n=11; AChR antagonists, 1.19 ± 0.09, n=8; unpaired t-test, t=2.975, df=17, **p=0.0085). **G.** Top, photomicrograph depicting the recording area in the habenula of ChAT::ChR2 mice. Bottom, experimental strategy for testing the role of nicotinic receptor signaling in endogenous ACh effects on MHb neural activity. In the presence of 4AP and iGluR and GABAR antagonists cocktail, light stimulation will facilitate ACh release while cholinergic neurons are recorded under current clamp in whole-cell mode in the presence or absence of mecamylamine (Mec) to block nicotinic receptor signaling. **H.** Representative trace before during and after light stimulation to induce a train of APs in MHb cholinergic neurons from ChAT::ChR2 mice slices (20 Hz, 5 sec, duration depicted by blue vertical lines) in the absence (top) and presence (bottom) of nAChR antagonist (Mec, 3 μM). 30s sweeps were acquired for 10 min. Dotted rectangle indicates the specific region used for power spectrum analysis (10 sec) for all cells. Scale bar: 2 sec, 10 mV. **I.** (Top) Power change (10–1000 Hz range, 10Hz interval) before and after Mec was plotted as a function of frequency. After Mec, power decreased (Repeated 2-way ANOVA, interaction frequency x treatment, F(99,594) = 2.725, p<0.0001; n=7 cells). (Bottom) P-values plotted as a function of frequency from analysis of power spectrum in panel (I). Blue dotted line indicates p=0.05 (paired t-test, df=6).

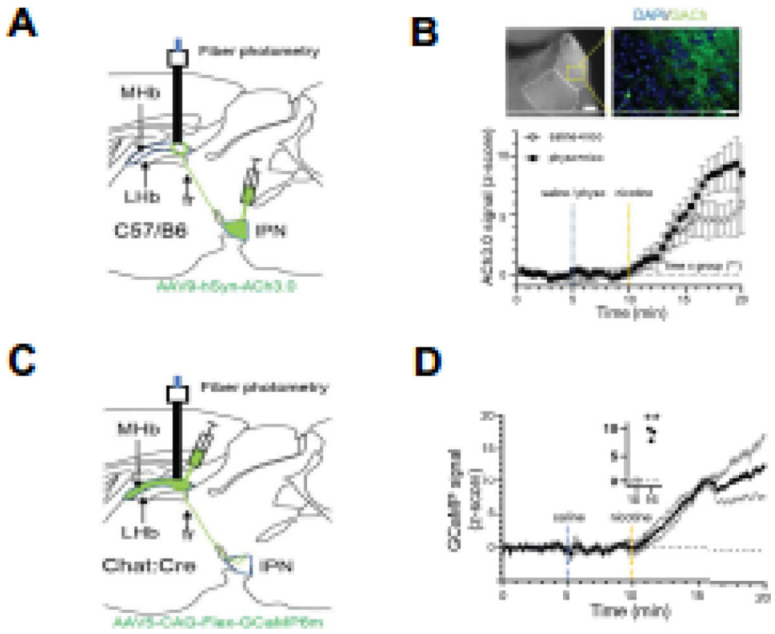

Figure 2. Detection of endogenous ACh in mouse habenula via an ACh sensor.

A. Top, experimental strategy for ACh3.0 expression in MHb and in vivo detection of ACh in MHb. AAV9-ACh3.0 was injected into the IPN of C57Bl/6J mice and fiber probe implanted in MHb. Right, representative photomicrograph depicting MHb and magnified area (dotted square) that depicting ACh3.0 expression. Scale bar: 100 μm (left), 20 μm (right).

B. Z-scored 465 nm ACh signal in MHb at baseline, after saline/physostigmine pre-injection, and after nicotine injection (saline+nicotine, n=4; physostigmine+nicotine, n=5; repeated 2-way ANOVA, time x group interaction, $F(39,273)=1.754$, $p=0.0055$). **C.** Experimental strategy for in vivo activity analysis of MHb in response to nicotine. **D.** Z-scored 465 nm GCaMP signal in MHb at baseline, after saline and after nicotine injection (n=3). Inset: before (10 min) and after (16 min) nicotine (10 min, 0.13 ± 0.92; 16 min, 9.90 ± 0.72; n=3; paired t-test, $t=19.93$, $df=2$, $p=0.0025$).

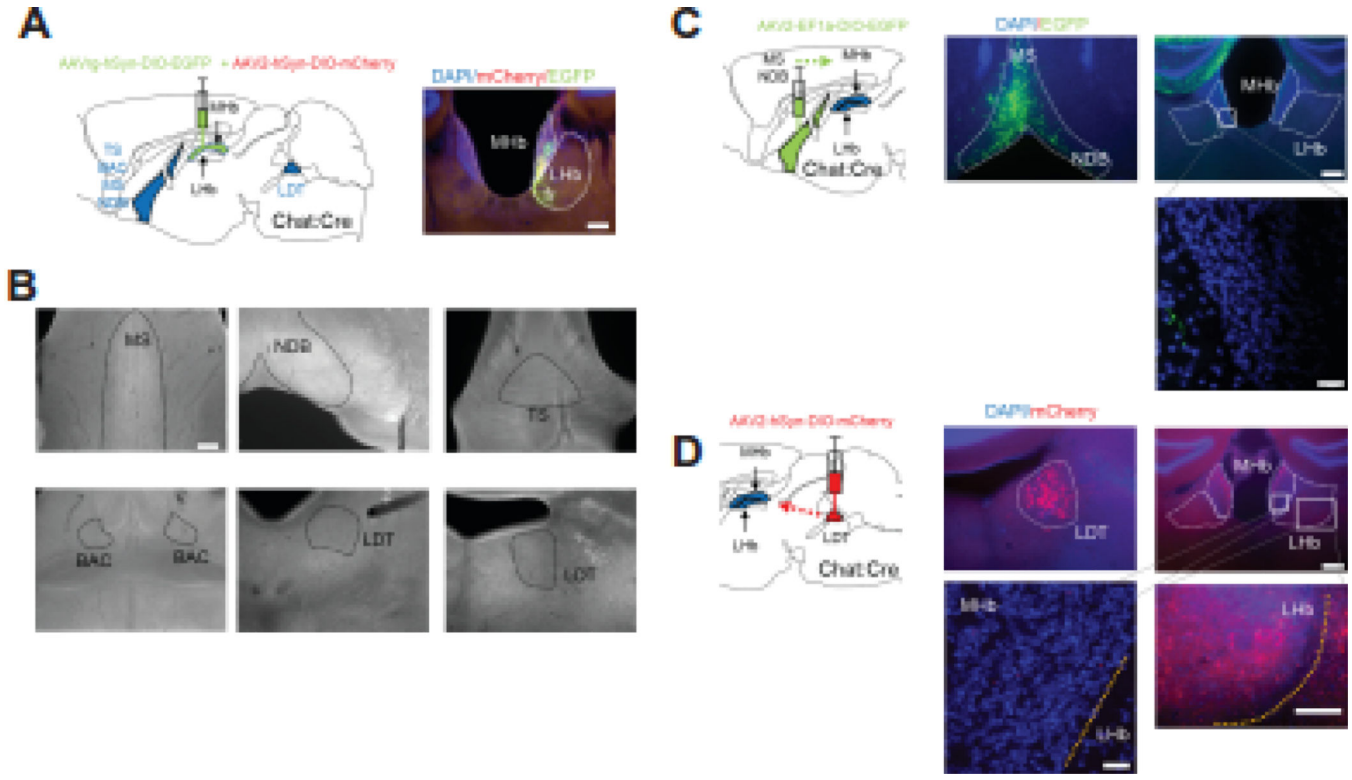

Figure 3. Viral tracing of potential cholinergic inputs to MHb.

A. Experimental strategy for retrograde labeling of cholinergic inputs to the MHb. AAVrg-hSyn-DIO-eGFP was co-injected into the MHb of ChAT::Cre mice with AAV2-hSyn-DIO-mCherry as an anterograde injection marker. Right, photomicrograph of the injection site depicting eGFP and mCherry expression in MHb (dotted line). Scale bar: 200 μm. **B.** Representative images of hypothesized brain areas that send cholinergic projections to MHb including medial septum (MS), nucleus of diagonal band (NDB), triangular septum (TS), bed nucleus of anterior commissure (BAC), and laterodorsal tegmental nucleus (LDT). Note that retrogradely labeled cells were not detected in any of the anticipated brain regions. Scale bar: 200 μm. **C.** Left, strategy for anterograde tracing of cholinergic neurons in MS and NDB of ChAT::Cre mice. Middle, eGFP expression in neurons in medial septum and NDB after AAV2-EF1a-DIO-EGFP injection. Right, eGFP signal from axons were detected in hippocampus, but not MHb. Scale bar: 200 μm (top), 20 μm (bottom). **D.** Left, strategy for anterograde tracing of cholinergic neurons in the LDT of ChAT::Cre mice. Middle, mCherry expression in neurons of the LDT after AAV2-hSyn-DIO-mCherry injection. Right, mCherry signal from axons was not detected in MHb. Scale bar: 200 μm (top right), 20 μm (bottom left), 100 μm (bottom right).

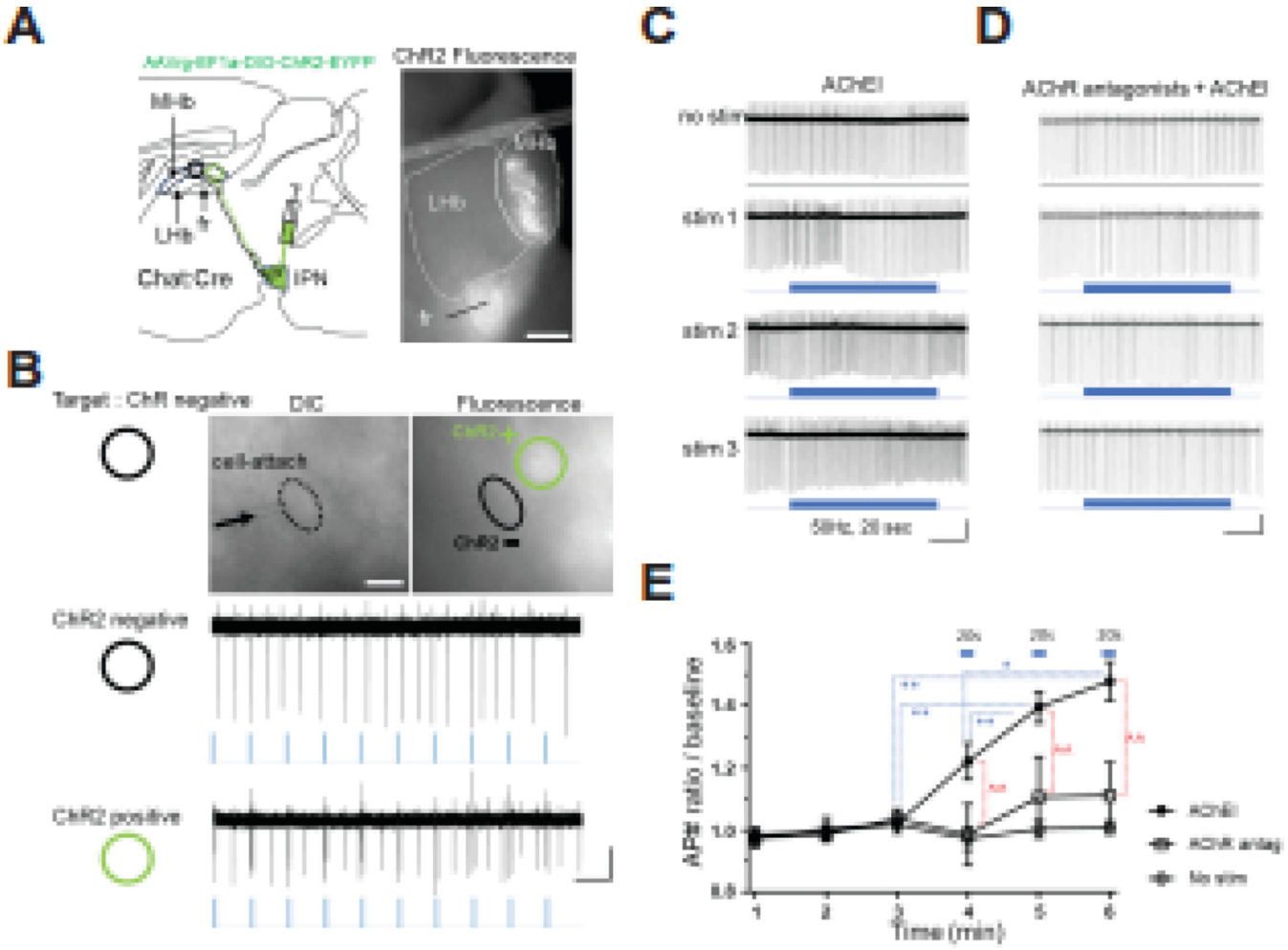

Figure 4. ACh drives feed forward activation of MHb cholinergic neurons induced by optic stimulation.

A. Left, diagram of experimental strategy. Retrograde ChR2 virus (AAVrg-EF1a-DIO-ChR2-EYFP) was injected into the IPN of Chat::Cre mice resulting in retrograde expression in a portion of MHb cholinergic neurons. Right, photomicrograph of epifluorescence signal from a Chat::Cre habenula slice demonstrating ChR2 expression in MHb and FR. Scale bar: 200 μm. **B.** Top, DIC and fluorescence image (60x objective) of a cell-attached ChR2-negative MHb neuron and a ChR2-positive MHb neuron. In addition to fluorescence, test light stimuli (2 pulses at 20Hz, 10 times at 1Hz) distinguished “ChR2-negative” cells (middle) from “ChR2-positive” cells (bottom). ChR2-negative cells were recorded for experiments in panels C-E. Scale bar: 10 μm (image), 1 sec, 10 pA (bottom). **C-D.** AP traces from cell-attached recording before and during 3 consecutive stimulations (50 Hz, 20 s, blue bars) in ChR2-negative MHb neurons in the presence of AChEI (**C**) or AChEI + AChR antagonists (**D**). Scale bar: C: 5 sec, 50 pA, D: 5 sec, 100 pA. **E.** Summed average of AP number ratio over baseline each minute from experiments shown in panels C and D. AChR antagonists with AChEI reduced the light-induced firing change (repeated 2-way ANOVA, interaction time x group, $F(10, 100)=4.424$, $p<0.0001$, n=10 (AChEI), 8 (AChR antag), 5 (No stim); multiple comparisons (Tukey test) at 4 min (AChEI, 1.22 ± 0.06; AChR antag,

0.99 ± 0.10; No stim, 0.97 ± 0.04; AChEI vs AChR antag, p=0.0111; AChEI vs No stim, p=0.0225; AChR antag vs No stim, p=0.9896), at 5 min (AChEI, 1.40 ± 0.05; AChR antag, 1.11 ± 0.13; No stim, 1.00 ± 0.03; AChEI vs AChR antag, p=0.0014; AChEI vs No stim, p=0.0001; AChR antag vs No stim, p=0.5358), at 6 min (AChEI, 1.48 ± 0.06; AChR antag, 1.11 ± 0.10; No stim, 1.01 ± 0.02; AChEI vs AChR antag, p<0.0001; AChEI vs No stim, p<0.0001; AChR antag vs No stim, p=0.5336)). Light stimulation increased firing in AChEI condition (repeated 1-way ANOVA, F(2.779,25.01)=27.74, p<0.001; multiple comparisons (Tukey test), 3min vs 5 min, p=0.0021; 3min vs 6min, p=0.0020; 4min vs 5min, p=0.0034; 4min vs 6min, p=0.0120), not in AChR antag (F(2.299,16.1)=0.7301, p=0.5151) and in No stim (F(2.334,9.337)=0.5171, p=0.6388) condition. *, ^ for p<0.05, **, ^^ for p<0.01.